Physics and applications of squid-inspired jetting

View the article online for updates and enhancements.

Physics and Applications of Squid-inspired Jetting

Qiang Zhu[a] and Qing Xiao[b,1]

[a]Department of Structural Engineering, University of California, San Diego, La Jolla, CA 92093, United States of America

[b]Department of Naval Architecture, Ocean and Marine Engineering, University of Strathclyde, Glasgow, G4 0LZ, United Kingdom

Abstract

In the aquatic world jet propulsion is a highly successful locomotion method utilized by a variety of species. Among them cephalopods such as squids excel in their ability for high-speed swimming. This mechanism inspires the development of underwater locomotion techniques which are particularly useful in soft-bodied robots. In this overview we summarize existing studies on this topic, ranging from investigations on the underlying physics to the creation of mechanical systems utilizing this locomotion mode. Research directions that worth future investigation are also discussed.

## 1. Introduction – inspiration from nature

Aside from undulatory and flapping motions of flexible body and body appendages, jet propulsion is another popular locomotion method utilized by a variety of aquatic invertebrates, including jellyfish, cephalopods (octopus, squid and cuttlefish), salps, and insect larvae [1] [2] [3] [4]. In terms of swimming capability there is little doubt that squid stands out as the champion among them [5].

Morphology and kinematics

As shown in Fig. 1a, a squid has a deformable body with an empty space in it called the mantle cavity, which acts as a pressure chamber. The cavity has two openings, a larger one called the mantle aperture and a smaller one called the funnel tube. The mantle wall consists mostly of two groups of muscles, radial muscles and circular muscles. During jet-propelled locomotion, there are two distinctive body deformations powered by these muscles with some help from the elasticity of the mantle wall [6] [7]: during refilling phase (i.e. the recovery phase) the mantle expands so that water is sucked into the mantle cavity through the mantle aperture at the rim (Fig. 1b); during jetting phase (the power phase) the mantle shrinks and pushes water out of the funnel tube (the mantle aperture is now closed) to form a jet. According to electromyographic (EMG) measurements [8], three distinctive muscle activities were found in this procedure: 1) contraction of the radial muscles leads to hyper-inflation of the chamber to prepare for an escape jetting; 2) contraction of the circular muscles powers the jetting; and 3) the refilling of the chamber is mostly activated via the elastic recoil of the mantle wall.

---

[1] Corresponding author: qing.xiao@strath.ac.uk
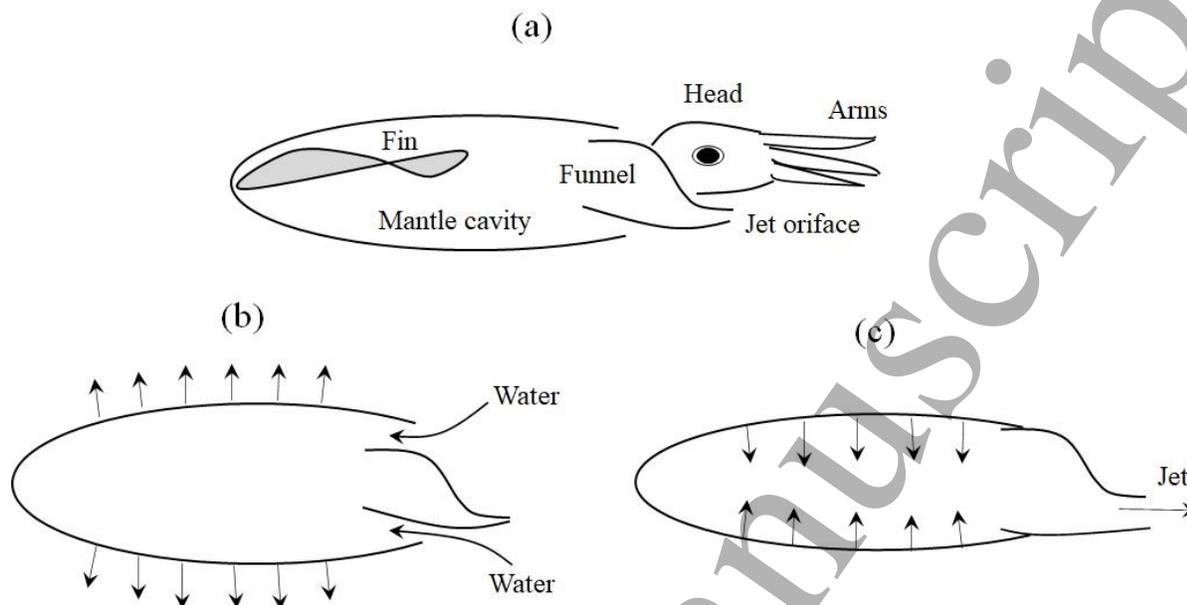
Figure 1. (a) A sketch of the structure of a squid. (b) During the refilling phase the body expands, and the mantle aperture is opened to let water into the mantle cavity. (c) During the jetting phase the body shrinks, the mantle aperture closes, and the funnel tube is opened to let water out. This figure is adopted from [9] (with permission of AIP Publishing), which was originally drawn (with some modifications) based on illustrations in [10] [11].

Swimming performance: speed and maneuverability

As pointed out by Bi and Zhu [12], the aforementioned jet propulsion mechanism via discharging and refilling of a pressure chamber is particularly suitable for soft-bodied creatures to achieve high swimming speed since during the power phase the wall of the chamber sustains mostly tension (rather than bending) load (see Fig. 2), which is easier for muscles to bear. Indeed, the most notable characteristic of squid is its impressively high swimming speed despite its lack of structural stiffness. According to measurements, the peak speed of *Loligo opalescens* is around 10 mantle lengths per second [13], and smaller ones such as the larvae of *Loligo vulgaris* reaches a bursting speed of 25 body lengths per second [5].

With the capability of ultra-high-speed bursting, some species of squids (e.g. *Ommastrephidae*, *Sthenoteuthis pteropus*, *Dosidicus gigas*, *Illex illecebrosus* and *Loligo opalescens*) are able to launch themselves out of water [14] [15] [16]. Once airborne, the remaining water in the pressure chamber is ejected for further acceleration so that the speed can reach 37 body lengths per second [15]. By spreading their fins for better aerodynamic performance, squid have been reported to glide as far as 33 meters (about 250 mantle lengths) in air [14].

Another notable feature is that the funnel tube, which serves as a nozzle during jetting, is able to point towards almost any direction so that changes in swimming direction can be achieved through

2

thrust vectoring. This is expected to be a highly effective direct-force-enabled way of maneuvering.
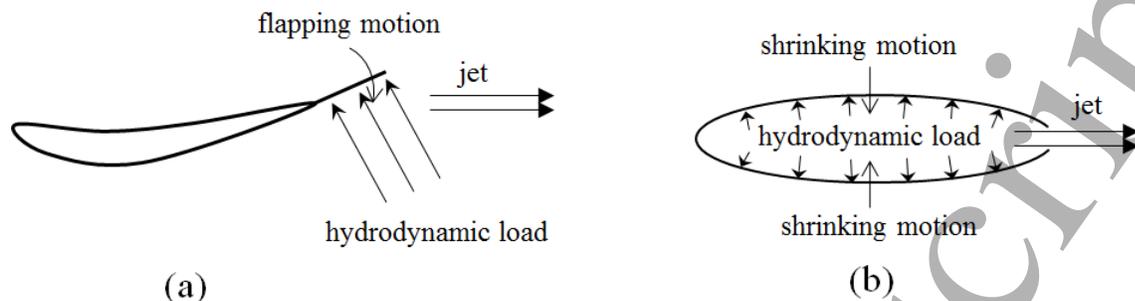
Figure 2. (a) In fish swimming the hydrodynamic load is often localized (e.g. on the caudal fin) and it induces mostly a bending load. (b) In squid jetting the hydrodynamic load is distributed on the mantle wall and during the power phase it induces tension in the wall. This figure is reproduced from [12] with permission of IOP Science.

Swimming performance: efficiency

In comparison with the undulatory and fin-activated locomotion methods of fish and marine mammals, the jet propulsion mode utilized by squid and other cephalopods were believed to be inherently low in efficiency since they rely on high speed jet to create thrust and a relatively large portion of the kinematic energy of the jet may be wasted [17] [18] [19]. This assumption seems to be supported by experimental measurements. For example, it was pointed out by Webber and O'dor that to reach half the speed of the average fish the best performing squid may use twice the energy [20] (also see [21]).

However, as pointed out by Linden and Turner [22], there is no guarantee that these measurements were conducted in swimming conditions that optimize the propulsive efficiency. Indeed, based on the reported data many of the measurements (e.g. [10] [23]) were done when the stroke ratio is much higher than the value known to produce the `optimal' vortex wake for best efficiency (see Section 2.1). Therefore, the results are not representative of the performance of squid. It is also implied that squid do not always swim at the most efficient mode. This has been confirmed by experiments using Digital Particle Image Velocimetry (DPIV) to record the near-body flow fields around live squids, in which multiple jetting modes corresponding to different ranges of stroke ratio have been found [24].

According to a more recent experiment [25], the propulsive efficiency of small squid (1mm in mantel length) is around 20%. For larger squid with around 1cm in length, the efficiency rises to 40%. In the low Reynolds number regime (O(1-100)) these animals act in, these numbers do not appear to be particularly low.

One of the difficulties in assessing energetics of squid-like jet propulsion is how to determine the propulsive efficiency, i.e., the ratio between the *useful power* (i.e. the power to overcome the drag force) and the *total power expenditure*. Traditionally, there exist three different ways to calculate the efficiency [10]:

1) Froude efficiency $= 2V/(V + V_j)$, where V is the swimming speed and V_j is the jet speed, i.e. the speed of the flow relative to the propeller.

2) Jet-period efficiency $= 2VV_j/(V^2 + V_j^2)$. This definition concentrates on the time when there is a jet going on so that it coincides with the efficiency of a rocket.

3) Whole-cycle efficiency $= 2VV_j/(2V_R V + 3V^2 + V_j^2)$, where V_R is the flow speed into the squid during refilling. Unlike the other two definitions of efficiency, the whole-cycle efficiency takes into account the energy spent to refill the body.

Nevertheless, all these definitions of propulsive efficiency are based on the simplified approach of ideal and steady flow. They are, however, convenient to be used in interpretations of experimental data since no detailed knowledge of the dynamical process and flow field is required.

For a more comprehensive evaluation of propulsive efficiency, it is necessary to separate the drag force F_D and the thrust force F_T on the body so that the efficiency is obtained as $F_T V/P$, where P is the power expenditure. In the context of squid-like jetting, there have been two proposed methods to achieve thrust-drag decomposition. These are:

1) *Thrust-drag decomposition for a steady rigid swimmer* [26] [27]: In this approach both the swimming speed of the body and the jet speed are constant. After self-propelled swimming state is established, the hydrodynamic force on the solid body is calculated via a Computational Fluid Dynamics (CFD) approach, which is assumed to be the drag force. In the steady state this drag force equals the thrust provided by the jet.

2) *Thrust-drag decomposition for an unsteady deformable swimmer* [28] [29]: This study considers a deformable body with an empty chamber in it. During cyclic deformations of the body the chamber is discharged and refilled periodically. By considering the flow fields both inside and outside of the deformable body, it is suggested that the hydrodynamic force on the inner side of the chamber is the source of thrust [28]. Through control volume analysis it was found that this force had three components: the flux momentum at the nozzle, the normal stress at the nozzle, and the inertia effect of fluid inside the chamber. All these components are obtained numerically so that the instantaneous thrust on the body is determined [28]. This work was later extended to the free-swimming scenario, in which one additional thrust component due to the added-mass effect of outside flow is added (see Section 2.2) [29].

Another frequently used method to quantify energy efficiency is the *Cost of Transport* (CoT), defined as the energy expenditure per unit distance of swimming. This parameter does not rely on thrust-drag decomposition so that it is easier to be applied. Indeed, it is widely used in cases where energy expenditure is readily obtained, for example in experiments with live creatures in which the energy expenditure can often be metabolically estimated. However, this definition only works in self-propelled swimming cases, whereas a large portion of the existing experimental or numerical studies of squid-like jetting is in the tethered mode. Besides, the original definition of this parameter is not dimensionless. There are proposed methods to normalize it, e.g. by defining it as the ratio between the energy expenditure and the swimming distance times the body weight.

As demonstrated in Fig. 3, in the rest of the paper we will review the existing experimental, analytical, and numerical studies about the key characteristics of squid-inspired jet propulsion, as well as efforts to imitate these characteristics in artificial systems.
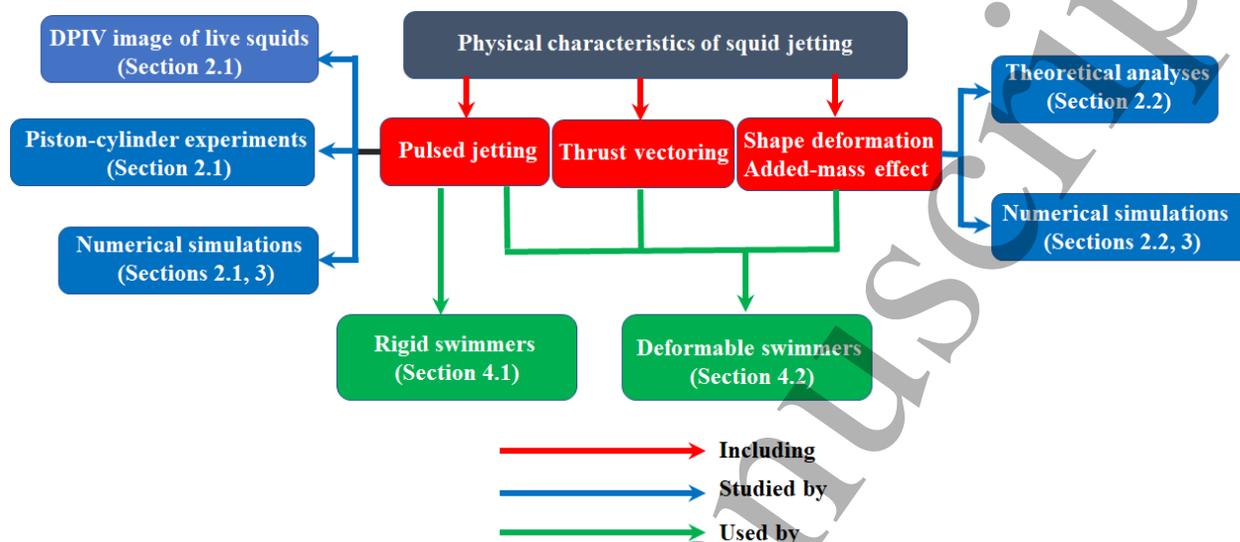
Figure 3. A graphical summary of the key characteristics of squid-like swimming, the existing studies to understand the underlying physics, and efforts to imitate these characteristics in artificial systems.

2. Underlying physics

Squid-like jet propulsion, including the jet-propelled locomotion mechanism of squid-inspired swimming systems, is a complicated process involving morphology, physiology, material science, fluid dynamics, structural dynamics, fluid-structure interactions, and sensing/controlling. We hereby review studies on two topics in fluid dynamics that play critical roles in this process. One of them is the dynamics of a single jet flow with finite duration. The other is the inertia effect of the surrounding flow field.

2.1 Physics of pulsed jets

Discovery of the formation number and its effects

During jet propulsion a significant portion of the thrust force on the body is generated by the repulse from the jet. In the literature the dynamics of this jet is often studied by using the idealized jet created by a piston in a cylindrical tube. If the volume of fluid discharged in a single jetting is $\forall$ and the nozzle is circular with diameter D, the discharged fluid can be imagined as forming a cylindrical jet plug with diameter D and length $L = \forall/(\pi D^2/4)$. The aspect ratio of this jet plug L/D, which corresponds to the stroke ratio in the scenario of a piston-generated jet (see Fig. 4), is an important dimensionless parameter that determines the evolution of the vorticity wake and the performance of the system in force generation.

In one of the pioneering studies, Gharib et al. experimentally examined the jet flow created by the piston-cylinder device [30]. The key finding is that there exists a critical value of the stroke ratio

*L/D~*4, which is called the *formation number*. When the stroke ratio is below that number, the leading vortex ring remains connected to the jet and its circulation keeps on growing with time. If the stroke ratio is beyond this number, however, a sequence of smaller vortex rings are generated along the jet. These vortices separate the leading vortex ring from the jet in a phenomenon called *pinchoff*. Subsequently the circulation of the leading vortex stops growing.
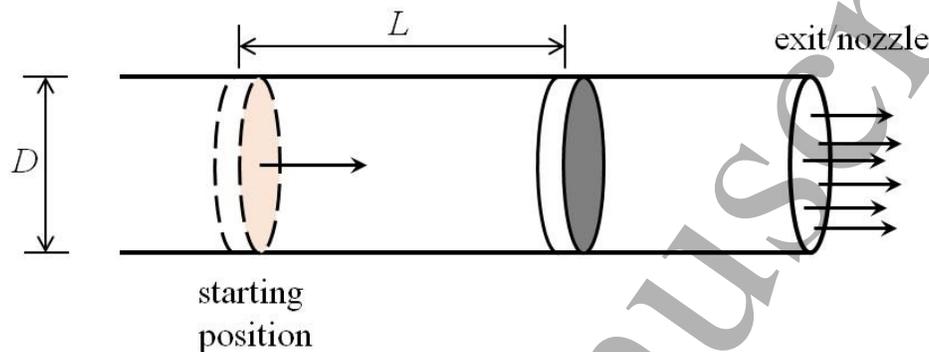
Figure 4. Definition of the stroke ratio *L/D* based on the piston-cylinder setup.

This phenomenon was later studied by using a numerical model [31]. Employing a commercial software package based on the finite element method to solve the axisymmetric Navier-Stokes equations, it was confirmed that the aforementioned phenomenon occurred in a variety of jet velocity distributions at the exit, time histories of jet speed (also referred to as the jet speed programs), and jet-related Reynolds numbers (i.e., the Reynolds number based on jet speed and exit diameter). A similar numerical study has been conducted recently, in which effects of both the starting vortex ring and the stopping vortex ring generated by jets with finite duration were examined [32].

In terms of force generation, the major source of thrust is the repulsive force from the jet, which can be expressed as the momentum flux at the exit, and it is related to the impulse of the wake. Another important contribution comes from the over-pressure at the exit [33]. With low Reynolds numbers the viscous normal stress at the exit also needs to be counted for [28].

A theoretical study has also been conducted to illustrate the underlying physics of pulsed jetting. By assuming that the circulation, impulse, volume and energy inside a cylindrical jet plug are all conserved when it rolls up into a vortex ring, it was discovered that there is a limiting aspect ratio (*L/D*) for this jet plug to form a single vortex ring, and the value is close to the formation number discovered experimentally [34]. Furthermore, it was suggested that the vortex ring formed at this condition contained maximum impulse, circulation and volume for a given energy input so that it was called the `optimal' vortex ring. The formation of the optimal vortex ring may be associated with maximum propulsive efficiency [35].

There is evidence that the jet propulsion method of squid swimming involves a large range of stroke ratios. Through DPIV illustration of the flow field around swimming squids, it was demonstrated that there were two distinctive modes in terms of the vorticity distribution, mode I and mode II [24] [36]. In mode I the wake is dominated by a single vortex ring, indicating that the

6

stroke ratio is below the critical value (the formation number). Mode II, on the other hand, is characterized by a long wake with a distribution of multiple vortices so that it corresponds to the case when the stroke ratio is above the formation number. Incidentally, the fin-activated swimming method of squid also features multiple modes in terms of vortex pattern in the wake [37]. This, however, is beyond the scope of the current study.

Effects of jet speed program and Reynolds number

Although in early investigations it was suggested that the formation number might be insensitive to factors such as the jet speed program and the Reynolds number [31], this conclusion was based on very limited number of cases and limited range of parameters (for instance, in Rosenfeld *et al*. [31] the range of Reynolds number is between 1250 and 5000, all within the intermediate Reynolds number regime). Later studies, however, suggested that the jet speed program might play an important role in determining the dynamics of the system. For example, Krueger and Gharib carried out experiments with two different velocity programs, negative-slope (deceleration) ramp and positive-slope (acceleration) ramp [38] [39]. It was found that the formation number in the second scenario is larger than the one in the first scenario.

The effect of Reynolds number has also been evaluated. With a robotic device swimming in a mixture of glycerin and water, Moslemi and Krueger [40] showed that in the low-Reynolds number regime (Re~$O(10^2)$) there was no clear pinchoff of the leading vortex ring. There is also much weakened effect of the maximum stroke ratio on the propulsive efficiency in comparison with cases at higher Reynolds numbers. Similarly, by using a piston-cylinder experiment, it was shown that at these Reynolds numbers with a constant jet speed program there did exist a critical stroke ratio (whose value is between 4 and 6) above which the leading vortex ring stopped growing [41]. There is, however, no secondary vortices being developed along the jet even after the leading vortex ring saturates so that the pinchoff of the leading ring from the jet is not pronounced. These observations have been confirmed numerically by using an immersed-boundary solver of axisymmetric Navier-Stokes equations [42]. In this numerical study various jet speed programs have been examined in the low Reynolds number regime. It was discovered that with some programs (e.g., a sinusoidal one) the circulation of the leading vortex ring did not saturate in stroke ratios as large as 15. Later numerical investigations confirm that at low Reynolds numbers the maximum stroke ratio has very small effect on the propulsion performance [28] [29].

Effects of background flow

Except for the starting jet at the beginning of an escape maneuver, the pulsed jetting is usually performed when there is a finite forward speed, or, equivalently, the presence of a background flow. The effect of such a uniform co-axial flow on the wake evolution behind a piston-cylinder device has been studied experimentally [43]. It was shown that the formation number decreased when the ratio between background flow speed and the jet speed increased. On the other hand, when the background flow is in the opposite direction of the jet, the pinchoff phenomenon can be delayed and the formation number increased [44]. A similar phenomenon was observed by Jiang and Grosenbaugh in their numerical simulation of this problem [45]. Their results also suggest that

7

when the background flow is sufficiently strong, there is no pinchoff of the leading vortex ring, or the leading vortex ring itself is highly deformed.

Effects of nozzle shape

In the piston-cylinder setup with a cylindrical nozzle the jet is uni-directional when it leaves the exit. However, the jets created by deformable bodies or jets from nozzles with different geometries contain not only longitudinal but also radial velocity components. A combined experimental and theoretical study has been carried out to illustrate the effect of non-zero radial velocity with several different exit geometries, an orifice without rectification, a tubular nozzle, and a converging nozzle [46]. By comparing the wakes generated by these exits, it was found that the converging nozzle, which induced a negative radial velocity at the exit, created a much stronger jet with higher circulation, impulse, and kinetic energy. More recently, Bi and Zhu simulated the thrust generation capacity of a deformable body with a nozzle affixed to it in a single discharge, which corresponds to the starting jet scenario [47]. Three different nozzle geometries were considered, tubular, diverging, and converging. For analysis the thrust is decomposed into its three components: momentum flux at exit, normal stress at exit (mostly from the over-pressure there), and time derivative of internal fluid momentum. Among them the second component, the over-pressure, is clearly affected by the nozzle geometry. Specifically, diverging nozzles decrease the over-pressure, whereas converging ones increase it. However, in the low Reynolds number regime the over-pressure only counts for a small portion of the thrust so that this effect is not pronounced in the overall thrust generation. In terms of energy efficiency, the diverging nozzle leads to less energy loss than the other two.

Interactions among multiple jets

The interaction among multiple pulsed jets has also been investigated. In experiments the dynamics of a system containing two pulsed-jet devices in a side-by-side configuration were examined [48] [49]. According to these studies the interaction between these jets reduces the overall thrust and efficiency. Furthermore, the performance of a system propelled by multiple jets in a more complicated configuration has been examined numerically [27]. With theoretical analysis it was pointed out that via asynchronous activation of multiple jets the oscillations in thrust generation may be diminished [50]. These studies are useful for a better understanding of the locomotion mechanism of creatures such as salps, and for developing underwater systems powered by multiple pulsed jetting devices.

2.2 Added-mass effect

The inertia effect of a solid object immersed in fluid contains two parts, the inertia of the object itself and the inertia of the surrounding fluid it carries (i.e., the added mass). Among these two the first part is usually constant whereas the second part can be time-dependent when the shape of the body is changing. This time-varying inertia has been shown to provide an additional source of thrust.

By using a deformable sphere as an example, Saffman demonstrated that it was possible to achieve persistent motion in an ideal fluid driven by shape deformation alone even if no circulation was

involved [51]. Later experiments show that a passively deformable object is able to hover in an oscillatory flow [52]. Although the process is complicated and involves the interplay among various mechanisms such as vortex shedding and wake dynamics, the time-varying added mass due to the shape change plays a non-negligible role. Inspired by this study, a numerical study was conducted regarding a two-dimensional deformable object by solving a vorticity-stream function type Navier-Stokes equation [53]. According to this work, a body with a fast increase in its aspect ratio in a process called *ratcheting* is capable of reaching high bursting speed. This process is reminiscent of the escape motion of creatures such as jellyfish or cephalopods. The underlying physics of phenomena like that was studied theoretically [54], where the motion due to the shifting of mass distribution of a deformable body is called the *recoil locomotion*.

Invoking conservation of momentum, the force exerted on the body due to added-mass effect is

$$-\frac{d(m_a V)}{dt} = -\dot{m}_a V - m_a \dot{V}, \tag{1}$$

where m_a is the added mass and V is the forward speed. The first term on the righthand side corresponds to the effect of the time-varying added mass (i.e., the frozen speed term) and the second term the frozen added mass term [55].

Considering a single deflation during the escape jetting, the lateral dimension of the body shrinks so that $\dot{m}_a < 0$, thus the `frozen speed' part of the added-mass-related force is positive. This force, in fact, is akin to the negative damping force since it is proportional to speed. The second term is the additional inertia effect, whose sign depends on the acceleration.

The added-mass effect can be alternatively viewed as a recovery of energy loss associated with the reduction of the added mass [56]. On the one hand, as the lateral dimension of the body shrinks part of the kinetic energy associated with its added mass is lost. On the other hand, the added-mass related force pushes the body so that a certain portion of the lost energy is recovered as the kinetic energy of the body. The ratio of energy recovery depends on how fast the shrinking happens as well as how much energy is dissipated in the process due to viscosity. To characterize this process a dimensionless number called the *shrinking parameter* σ^* is defined as $(\dot{a}_{max}/U)R_{e0}$, where $\dot{a}_{max}$ is the maximum shrinking speed, U is the characteristic flow velocity, and R_{e0} the Reynolds number at the beginning of the shrinking motion. Through numerical simulations of a shrinking object in tethered motion, it was discovered that in order for there to be sufficient energy recovered to produce net thrust σ^* has to be larger than 10. In a broader sense, through a combination of numerical simulations and theoretical models, Giorgio-Serchi and Weymouth pointed out that by carefully choosing the ratio between the shape change frequency and the natural frequency of a periodically deforming object, it is possible to completely overcome the viscous damping effect and generate sustained oscillations by the recovered kinetic energy from added mass [57]. In this work an analytical expression of the added-mass variation term has been formulated. Similar analyses have been conducted with respect to a self-propelled swimmer, in which the effects of the inertias of outside fluid and internal fluid have been incorporated into the model [58].

Following these studies, Bi and Zhu approximately calculated the additional thrust due to added mass by using the first term in the righthand side of Eq. (1) with the added mass m_a estimated

through simplified models [29] [59]. In a single deflation this term remains positive. In repeated deflation and inflation deformations, on the other hand, its sign oscillates – positive during deflation and negative during inflation. Since the forward speed *V* is usually larger during deflation the net effect of the contribution from this term to the thrust is positive. With this approach it was discovered that in free-swimming cases the added-mass-related thrust was significant if there was a large difference between the inflated and the deflated shapes [59] [60]. When the body deformation is relatively small, this force can be negligibly small in comparison with other components of thrust [29].

3. Numerical work

Unlike the large quantity of existing numerical studies of the dynamics of other aquatic locomotion modes, there are only a handful of studies about squid-like jet propulsion. These studies are listed below.

Simplified models

A coupled fluid-structure interaction model has been developed to study the dynamics of a squid-inspired soft-bodied robot [61] (see Section 4). The body of the robot is modelled as a thin shell enclosing an empty space that serves as the pressure chamber. The dynamics of the shell is formulated using the Reissner shell model. Following the actual design of the robot, the actuation is provided by a set of cables (also see [62]). The fluid dynamics, on the other hand, are incorporated through a simplified Morrison-type approach in which the fluid-dynamic force is considered as the combination of three effects, the drag, the added mass, and the thrust. Simplified models have been used to find the values of the force components.

Potential-flow-based boundary-element models (BEM)

A potential-flow-based numerical model was developed by Bi and Zhu [59]. Similar to the aforementioned simplified model, in this model the swimming system is depicted as a thin shell with a pressure chamber which can be discharged and refilled. The body deformation is prescribed, while the forward motion is calculated through Newton's equation. The fluid viscosity is not considered so that the fluid dynamics can be formulated with boundary integral equations [63]. The wake, which originates from the edge of the exit, is modeled as a thin shear layer and mathematically represented by distributions of dipoles. The strength of the newly shed wake is determined by the Kutta condition, while the wake elements shed earlier translocate downstream under the combined effect of the surrounding flow field and the induced velocity. Compared with models including viscous effects, this method is efficient since it does not discretize the fluid domain, although it can only be used in cases with large Reynolds numbers.

Immersed-boundary models (IBM)

In this model the Navier-Stokes equations are solved in a Cartesian mesh with a finite difference algorithm. A multi-block technique is used so that higher resolution is reached near the solid body with increased mesh density. The structural deformation is either prescribed or solved separately

10

via structural dynamics. The fluid-structure coupling is achieved through a penalty algorithm which ensures the consistency of velocity at the interphase.
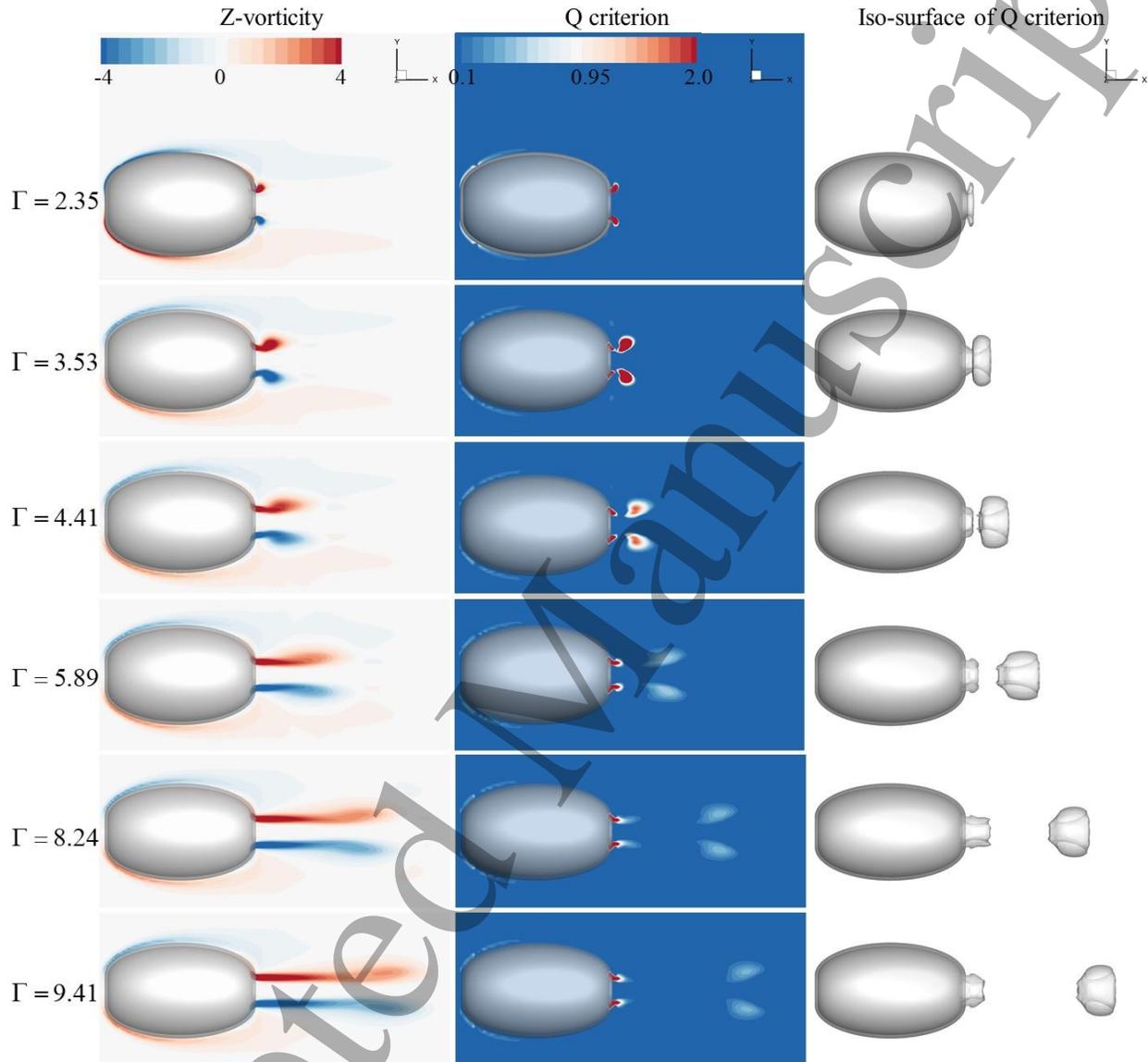
Figure 5. Evolution of the wake behind a squid-inspired swimmer with a constant speed background flow predicted by a 3D CFD model. Hereby the wake is visualized via the vorticity distribution in a plane of symmetry (left), the Q-criterion distribution in the same plane (middle), and the 3D iso-surface of Q criterion (right). Γ is the instantaneous stroke ratio. The maximum stroke ratio is 10.59. The ratio between the background flow speed and the peak speed of the jet flow is 0.42. This figure is reproduced from [64] with permission of AIP Publishing.

In two dimensions, the structure (hereby the mantle wall) is represented as a beam with finite bending stiffness but zero thickness. Mathematically it is formulated by using the nonlinear Euler-Bernoulli beam model. The actuation system includes a group of springs whose natural lengths can be changed. This model has been used to study the dynamics of the system in both tethered

[9] and free-swimming [12] cases. The Reynolds number in these studies is usually $O(1\sim 10^2)$. Interestingly, in both cases the wake is disturbed by a symmetry-breaking instability so that the system is not able to maintain straightline swimming for more than a few cycles. The source of instability is the interactions among vortex pairs in the wake. Incidentally, although this phenomenon is discovered in 2D simulations, in 3D cases there could also be instabilities due to interactions among vortices. For example, it has been illustrated through experiments with a piston-cylinder devices that the interaction between the leading vortex ring and the vortex ring in front of the piston could lead to instability and eventually turbulence [65].

An axisymmetric version of this model has also been developed. In this model the body is depicted as a zero-thickness shell, whose deformations are prescribed. Like the two-dimensional model, the axisymmetric model can also be applied to simulate tethered [42] or self-propelled [29] cases.

2D and 3D CFD models

Luo et al. created a two-dimensional CFD model of a squid-like swimmer [66]. In this model the body of the swimmer is simplified as part of a hemi-ellipse with an open end that serves as the nozzle. The fluid–structure interaction simulation is achieved by using an in-house flow solver based on the finite volume method (FVM) coupled with the open-source structural solver CalculiX. By performing the FSI study at high Reynolds numbers ($O(10^5)$), it is possible to examine how the system would behave in turbulent flow regime (hereby the two-equation $k - \omega$ model is invoked for turbulence modeling). To replicate a more biologically relevant system, in this study the active deflation of the mantle is actuated by an external force mimicking the function of the circular muscles and the passive inflation results from the release of the elastic energy in the mantle structure. A systematic study on the Reynolds number effect indicated that larger swimming speed could be achieved at higher Reynolds numbers, mainly due to the suppression of body-generated vortices near the outer body surface. Accordingly, the efficiency can also be increased by as much as 25%. Similar to the cases at lower Reynolds numbers [12] [9], symmetry-breaking instability is also observed, although it is initiated by the vortex interactions inside the chamber rather than in the wake.

A three-dimensional version of the model was also created [64] (see Fig. 5). The focus is on the near-body fluid field, vortex ring formation and jet propulsion performance with various background flow conditions. A single deflation deformation is considered. Different jet velocity programs were examined to determine their impacts on the evolution of jet vortex rings. Computational results suggest that the thrust generation due to jet is reduced at larger background flow speeds.

Axisymmetric CFD model

A CFD model was developed by Jiang and Grosenbaugh to study the dynamics of an elongated and axisymmetric body with a background flow [45]. Inside the body there is a cylindrical chamber with a moving piston in it. When this piston slides backwards a jet flow is generated at the exit of the chamber. The problem was numerically simulated by using the finite volume method through

12

the commercial software FLUENT. In later studies a similar numerical setup was used and solved with the same numerical approach, yet the jet was directly incorporated by imposing an outflow speed at the end of a solid body [26].

Multiphase CFD model

A multiphase CFD model was recently created to study the launch procedure of a squid from water to air [67]. This work is characterized by a realistic 3D geometry of a squid constructed using *Solidworks*. On the other hand, the body is modelled as rigid, and the jet is artificially prescribed. The fluid dynamics is solved by using the finite volume method via the commercial software package FLUENT. The Reynolds averaged Navier–Stokes (RANS) method is used for turbulent flow modeling. A volume of fluid (VOF) model is employed for the multiphase flow problem.

A summary of these models is shown in Table 1.

Model type	Fluid model	Flow regime	Structural model
Simplified [61] [62]	Morrison equation	N/A	Elastic shell actuated by cables
3D BEM [59]	BEM	Potential	Prescribed deformation
2D IBM [12] [9]	IBM	Laminar	Elastic beam activated by springs
Axisymmetric IBM [29] [42]	IBM	Laminar	Prescribed deformation
2D CFD [66]	FVM	Turbulent	Elastic beam activated by applied force and elastic recoil
3D CFD [64]	FVM	Laminar	Prescribed deformation
Axisymmetric CFD [26] [27] [45]	FVM	Laminar	Rigid (w/ or w/o moving piston inside)
3D Multiphase CFD model [67]	FVM and VOF	Turbulent	Rigid

Table 1. Summary of existing numerical models of squid-like jet propulsion.

4. Applications

4.1 Rigid-body mechanical swimmers

An early investigation of squid-inspired underwater robots was conducted by Krieg and Mohseni [68]. This was motivated by the idea of developing a new type of underwater jet thruster which may offer faster tracking and lower drag than typical propellor thrusters, while maintaining the thrust capabilities at zero forward velocity. The device was composed of a cavity with a moving wall on one side and an orifice on the other side. The cyclic motion of the moving wall leads to periodic ingestion and exclusion of fluid in and out of the cavity, creating synthetic jet in the wake so that there is zero net mass flux over an entire actuation cycle but a positive momentum flux. To characterise the thrust generation by this device, the main parameters controlling the jet and thrust were identified and examined through both experimental test and theoretical analysis. Their findings show that the thrust relies on the frequency, the size, and the pulsation time of the jet.

13

Trajectory tracking experiments also indicated that this device was able to rotate and swim sideways.

Moslemi and Krueger developed a similar underwater vehicle named *Robosquid* [69]. It comprises a piston, a cylinder, a nozzle, and a stepper motor contained within a streamlined housing. The reciprocating motion of the stepper motor results in the pulsed jet. To test its self-propelled motion performance, this robot was placed in a water tank supported by a mounting fin connected to a cart constrained to move linearly on an air track. The main objective was to study the dependence of its propulsive efficiency upon jet velocity program, pulsing duty cycle and maximum stroke ratio (within a range of 2–6). By measuring the thrust generation with a trapezoidal jet velocity program and a triangular one, it was found that higher propulsive efficiency was reached in the former case. To study the effects of Reynolds number upon the dynamics of this device, it was later tested in a mixture of glycerin and water so that the range of Reynolds number was reduced from 1300-2700 to 37-60 [40]. It was discovered that within this range of Reynolds number, the pinchoff of the leading vortex ring with a stroke ratio beyond the formation number did not occur, and the effect of maximum stroke ratio on the propulsive efficiency was not pronounced (see the discussion in Section 2.1). Moreover, by comparing the performances of steady-jet propulsion and pulsed-jet propulsion it was suggested that at lower Reynolds numbers pulsed jetting might be an efficient way of locomotion.

Another underwater vehicle was developed to examine the steady and unsteady pulse-jet propulsion of thrust generation and the role of vortex formation [70] (also see [71]). It has a conventional submarine profile with an anterior, water-flooded nose cone, a waterproof motor housing with attached hydrofoil support strut, a water-flooded inlet housing and a posterior exit nozzle connected to the inlet housing. Experiment was conducted using towing tank for the measurement of hydrodynamic forces. The wake was captured using DPIV. To complement the experiment study, an analytical model was developed focusing on the empirical measurements of vortex entrainment and added-mass dynamics in the near-wake. In the tethered swimming condition, a comparison between steady-jet and unsteady-jet scenarios indicates that the latter case is characterized by more rapid shear layer growth and larger-scale coherent vortex rings, while the former case creates a conventional turbulent jet with relatively uniform speed in the core flow. Results from self-propelled tests suggest that the ambient fluid entrainment in the unsteady propulsor plays more significant role in the near-wake structure relative to the steady propulsor. Overall, the unsteady-jet method leads to up to 70% performance improvement in terms of the Froude efficiency in comparison with the steady-jet propulsion.

Inspired by flying squid's unique capacity of fast takeoff into the air and glide above the water surface, Zufferey et al. developed a prototype aquatic-aerial robot [72]. The main challenge for such aquatic-aerial design is the significant density difference between air and water, which requires a rapid acceleration from underwater to air. The speed during this transition can be as high as 10 m/s. Unlike the device in [73] where high-speed jetting was driven by a pressurised flexible cavity/membrane, in this work the water jet is generated by a combustion process in which the acetylene gas generated by solid fuel burns inside a combustion chamber to push a pump, which produces the jet. Tests conducted in laboratory and outdoors revealed that this robot was able to achieve a maximum flight distance of 26m, rise to a maximum height of 8.3 m, and reach maximum thrust peak pressure, acceleration, and velocity of 7.8 bars, 110 m/s2, and 11 m/s, respectively. Experimental results, hereby the velocity and acceleration of the robot during the initial stages of flight, were reproduced by CFD analysis.

14

Novel actuation methods have also been proposed for pulsed-jet locomotion. For example, Tang et al. developed a swimming system utilising a dielectric elastomer actuator [74]. They pointed out that unsteady jet could be generated by the oscillation of a flexible membrane (hereby a membrane made of dielectric elastomer material) inside a cavity with one or more orifices on the wall. It has been demonstrated that this device could swim at a speed of 0.66 body length per second above the water surface by pulsed air jet, or at a speed of 0.43 body length per second underwater.

4.2 Deformable mechanical swimmers

A series of soft-bodied robot prototypes have been developed at the Scuola Superriore Sant's Anna Italy in collaboration with Ecoledes Minces de Nantes France, under the EU Commission in the frame of the CFD-OctoProp Project FP7 [75] [76] [61] (Fig. 6a). This new type of device consists of an elastic hollow shell made of elastomer material. The deformation of the shell is controlled by distributed cables, which are actuated by a DC motor. With activated shell collapse and auto-inflation process, self-propulsion with periodic motion of the robot is achieved. Experimental tests in a water tank indicate that propulsive performance heavily relies on the elastic response of the shell to the actuation cycle. Video recordings reveal that this system can reach a maximum velocity around 0.2m/s or 1.45 body length per second under the maximum DC motor frequency.
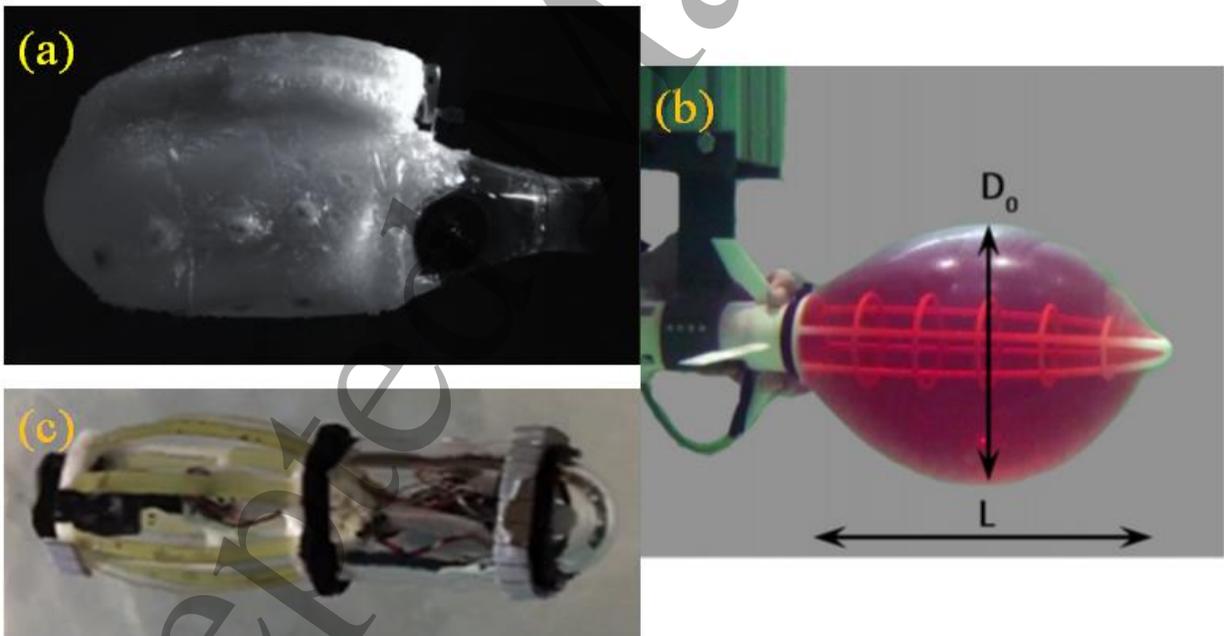

Figure 6. Examples of existing designs of deformable swimmers inspired by squids: (a) an elastic swimmer driven by motor and cables (reproduced from [61] with permission of IOP Science), (b) an ultra-fast swimmer driven by elastic energy stored in its skin (reproduced from [77] with permission of IOP Science), and (c) a deformable swimmer with elastic skin and ribs driven by motor with a slip-gear design (reproduced from [60] with permission of IOP Science).

A subsequent work by Giorgio-Serchi et al. [78] extended the above design to examine thrust maximizing using a soft actuator composed of an elastic hollow membrane fitted onto a rigid

compartment which contains a valve and a pump. During tests the system was held still, and the force generated with different nozzle configurations were measured to determine the turning moment due to thrust vectoring. Experiments demonstrated that passive deformation can be effectively utilized to control the thrust generation and power consumption. By tuning this, it is also possible to realize a wide range of swimming modes.

The study of Weymouth et al. [77] focuses on the jet propulsion during the start of the escape maneuver (Fig. 6b). A flexible hull swimmer was built using a rigid neutrally buoyant skeleton with an elastic membrane wrapped around it. The device is hyper-inflated with water, and then rapidly deflates to eject the water out through a nozzle to imitate the fast-starting behavior for escaping. Experiments indicate that the peak velocity of such soft device is above 10 body lengths per second (or 2.7 m/s). Unlike other devices, however, there is no refilling mechanism for this design so that it is not capable of continuous swimming.

A recent paper reports the development of a squid-like aquatic-aerial robot with soft morphing fins and arms to mimic flying squids in nature [73]. In their design, the fins and arms are made of silicone and actuated by a pneumatic system to induce inflation and deflation of flexible cavity so that fins spread in air and fold in water. Experiments conducted in wind tunnel and water tunnel prove the feasibility of this prototype in three scenarios, underwater swimming, surface breaking, and airborne gliding. Unfortunately, the reported data are limited to drag and lift forces. There is no quantitative result about locomotion performance.
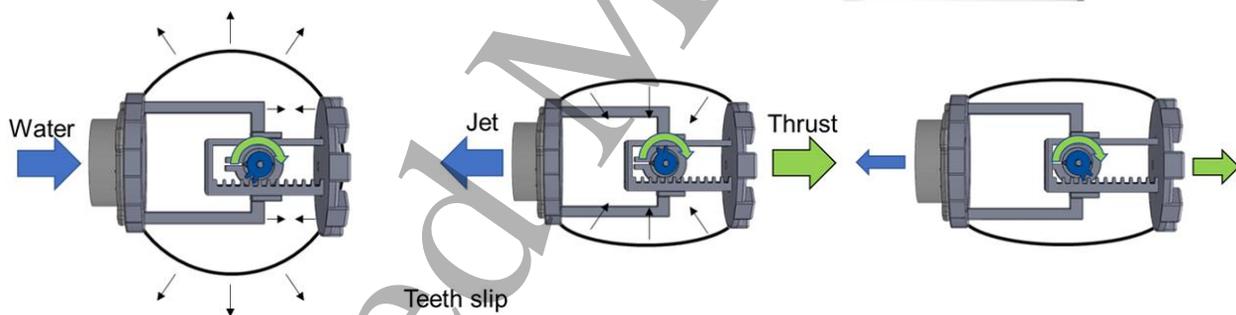
Figure 7. A hybrid activation system including a DC motor, a slip-gear system, and elastic energy storing/release system with elastic skin and ribs. In this design the gear is engaged during inflation (the left figure) so that the body deformation is driven by the motor. During deflation (the other two figures) the gear detaches and the elastic energy in the system is released. This figure is reproduced from [60] with permission of IOP Science.

Publication	Rigid or soft-bodied	Tethered or self-propelled	speed	Actuation method	Other notable characteristics
Krieg and Mohseni [68]	Rigid	Tethered	N/A	Mechanical actuator	

16

				driven by motor	
Moslemi and Krueger [69] Ruiz et al. [70],	Rigid	Tethered or self-propelled	N/A	Mechanical actuator driven by motor	
Zufferey et al. [72]	Rigid	Self-propelled	Peak speed~ 11m/s in air	Chemical reaction	Aquatic-aerial robot
Tang et al. [74]	Soft	Self-propelled	Average speed ~0.66BL/s above the water surface ~0.43BL/s underwater	Dielectric elastomer actuator	Aquatic-aerial robot
Giorgio-Serchi et al. [75] [76] [78]	Soft	Self-propulsion	Peak speed~ 0.2m/s (1.45 BL/s)	Distributed cables, actuated by motor; or elastic material with a pump	Capable of off-axis jetting for thrust vectoring
Weymouth et al. [77]	Soft	Self-propelled	Peak speed~ 10BL/s	Flexible material	
Hou et al. [73]	Soft	Tethered	N/A	Silicone and actuated by a pneumatic system to induce inflation and deflation of flexible cavity	Capable of underwater swimming, surface breaking, and airborne gliding
Christianson et al. [60]	Soft	Tethered or self-propelled	Average speed ~0.54BL/s peak speed ~0.94BL/s	A hybrid activation system including a motor, a slip-gear system, and elastic energy storing/release system with elastic skin and ribs	Capable of turning via thrust vectoring
Bujard et al. [79]	Soft	Self-propelled	0.98 BL/s	Solenoid actuator	High efficiency

| Yang et al. [80] | Soft | Tethered | 0.2 BL/s | A double-spool system driven by motor | Origami-inspired skin design |

Table 2. Key characteristics of existing squid-inspired locomotion systems.

Another squid-inspired pulsed jetting swimmer was developed and tested by Christianson et al. [60] (Fig. 6c). The basic design is characterized by a pressure chamber enclosed within an elastic skin strengthened by deformable ribs. The body expansion and deflation are created by a hybrid active-passive mechanism, in which the inflation motion is activated by a DC motor via a slip-gear system and the deflation is triggered passively by the release of elastic energy stored in the skin and the ribs (see Fig. 7). Both tethered and self-propelled swimming scenarios were examined. During self-propelled swimming the peak swimming speed of this system is around 0.94 body length per second and the average speed is around 0.54 body length per second. Similar to previous studies [78], effects of off-axis jets have been studied. The device demonstrated the ability of small radius turning maneuver by thrust vectoring. The actuation system is mechanically simple, reliable, and powerful. On the other hand, due to the design of the slip-gear device the motor is powered over the whole inflation-deflation cycle yet only engaged during inflation, which leads to waste of energy input. There is significant space for improvement in terms of energy efficiency.

In the study by Bujard et al. [81] (also see [79]), the possibility of performance enhancement via resonance is explored. Towards this end, a squid-like robot was designed following the concept of a spring-mass oscillator. The robot is composed of an umbrella-like system with several ribs arranged axi-symmetrically, which are covered with a flexible membrane. The radial expansion and contraction are controlled by an actuator. To overcome the force generated by the stretchable membrane, a piston is installed along the axis of the robot. Deformations are achieved via the balance among the environmental fluid force, the tension force of spring and the elastic force of structure. Experimental results were analysed with three main parameters, i.e., the self-propelled swimming speed, the quasi-steady propulsion efficiency, and the mechanical cost of transport. The main conclusion is that an effective use of mechanical resonance leads to improved propulsive performance. In the self-propelled condition, this robot swims at a preferred Strouhal number for optimal performance, which are reminiscent of similar findings from fish swimming. A notable feature of this device is its high propulsive efficiency of 56%. The recorded CoT (normalized by the dry weight of the body) is 0.087, which is comparable to that of jellyfish.

More recently, in the paper by Yang et al. [80], an origami-inspired swimming robot was proposed. In comparison with the aforementioned soft-bodied swimmers relying on elastomeric skins for shape change, this novel design might be more conveniently fabricated and assembled. The device is constructed with a ball origami counterpart. Periodic change in cavity volume is controlled via a motor and tendons. A water tank test using high resolution videos proved that this design could reach a swimming speed of 6.7 cm/s (or 0.2 body length per second). Tests with variable actuation frequency and cavity shape deformation lead to the conclusion that larger deformations and lower actuation frequencies could result in a reduction of COT.

A summary of the existing squid-inspired locomotion devices and their key characteristics is shown in Table 2.

5. Conclusions and future directions

18

Inspired by the locomotion capacity of squid in the jet propulsion mode, extensive experimental, theoretical, and numerical studies have been conducted to investigate the underlying physics of pulsed jetting. These studies illustrate that a dimensionless parameter, the stroke ratio, plays an important role in determining the wake characteristics and propulsive performance. Other factors, such as the Reynolds number, the jet speed program, the nozzle shape, and the background flow, also affect the dynamics of the system. In addition to the repulsive effect of the jet, the inertia effect of the flow has also been found to contribute to thrust generation.

Numerical models have been developed to simulate the fluid-structure interaction problems involved in both tethered and self-propelled scenarios. These models include 2D, axisymmetric, and 3D depictions of the physical problem in different ranges of Reynolds numbers. They are not only helpful in understanding the physical mechanisms but also useful in identifying the physical parameters related to optimal locomotion performance.

In the application side, various designs of squid-inspired swimmers with both rigid and deformable bodies have been developed and tested. These prototypes demonstrate the feasibility of this locomotion method as well as its potential advantage in swimming speed, efficiency, and maneuverability.

On the other hand, most of the existing squid-inspired underwater systems swim around (or below) 1 body length per second, which is one order of magnitude slower than their natural counterparts. One exception is the device developed by Weymouth et al. [77], whose peak speed is comparable to the one a squid can reach in nature. This design, however, relies on stored elastic energy for its impressive bursting speed. There is no mechanism to refill the pressure chamber so that the distance it travels is very limited. It is thus clear that there is significant space for improvement for this type of bio-inspired swimmers.

Aside from improvements in activation and controlling systems, on the theoretical side, it is necessary to illustrate the wake dynamics, force generation capacity, and energetics of pulsed jetting over a wide range of jet speed programs and Reynolds numbers. In particular, the role of stroke ratio on the propulsion performance under various conditions needs to be clarified. Another topic that has not been studied extensively is the interplay among the fluid dynamics, the structural dynamics, and actuation/controlling systems.

An important part of the energetics of the system is the energy expenditure to refill the pressure chamber [82]. Existing designs often feature a single opening which functions as both the inlet for refilling and the outlet for jetting. Subsequently the refilling flow is in the opposite direction of the jet so that its kinetic energy does not contribute to the jetting process. To reduce the energy waste during refilling, Bi and Zhu propose to slow down the inflation phase so that the speed of the flow entering the pressure chamber is reduced [29]. This method, however, also reduces the forward speed since it elongates the duration of the inflation phase, during which little thrust is generated. On the other hand, nature has provided a few possible solutions for this issue. For example, in squid swimming the refilling and discharging of the pressure chamber (the mantle cavity shown in Fig. 1) are through different openings – during refilling water is sucked in through the mantle aperture, whereas during discharging the water leaves through the funnel tube. The mantle aperture

has much larger area than the funnel tube so that the speed (and subsequently the kinetic energy) of the flow into the chamber is relatively small and less energy is wasted in this process. This is the method used by Giorgio-Serchi et al. in the design of their underwater vehicle [75]. Another option is to put the inlet and outlet at the opposite ends of the body, as suggested in [59]. This design may lead to a mostly uni-directional flow in the pressure chamber so that the kinetic energy of the inflow can be used in the jetting process. This appears to be the strategy utilized by salps [83] [84]. There is, however, no existing study about the dynamics of the complete deflation-inflation cycle in this approach and the energetics is not clear either.

Another topic that requires further investigation is the ability of turning maneuver via thrust vectoring. In some existing designs off-axis nozzles are used to change the direction of the jet flow for direct-force control [60] [78]. However, these nozzles are prefabricated rigid ones that are not adjustable during operation. A swimmer with steerable nozzle has been developed and its maneuverability has been demonstrated in tests [85]. Adjustable nozzles with more degrees of freedom, such as those activated by shape memory alloys [86], will be useful for this purpose. Moreover, theoretical, numerical, and experimental studies are needed to examine the underlying physics and the effectiveness of this maneuvering method. Although the evolution of the vorticity field created by jets into cross flow has been studied extensively through experiments [87] [88] [89] [90], there is little existing knowledge about the force generation capacity of these jets. Such knowledge will be critical in the development of highly efficient maneuvering methods based on pulsed jetting. Future studies are necessary.

Acknowledgements

References

[1] S. Vogel, Life in Moving Fluids. The Physical Biology of Flow, 2nd, Ed., Princeton, NJ,: Princeton University Press, 1994.

[2] S. Vogel, Comparative BiomechanicsL Life's Physical World, Princeton, NJ: Princeton University Press, 2013.

[3] B. Gemmell, J. O. Dabiri, S. Colin, J. Costello, J. Townsend and K. Sutherland, "Cool your jets: biological jet propulsion in marine invertegrates," *J. Exp. Biol.,* vol. 224, p. jeb222083, 2021.

[4] L. Madin, "Aspects of jet propulsion in salps," *Can. J. Zool.,* vol. 68, pp. 765-777, 1990.

[5] J. Gosline and M. DeMont, "Jet-propelled swimming in squids," *Sci. Am.,* vol. 252, no. 1, pp. 96-103, 1985.

20

[6]   D. Ward, "Locomotion function of the squid mantle," *J. Zool. Lond,* vol. 167, pp. 449-487, 1972.

[7]   D. Ward and S. Wainwright, "Locomotion aspects of squid mantle structure," *J. Zool. Lond.,* vol. 167, pp. 437-449, 1972.

[8]   J. Gosline, J. Steeves, A. Harman and E. Demont, "Patterns of circular and radial mantle muscle activity in respiration and jetting of the squid Loligo Oplescens," *J. Exp. Biol.,* vol. 104, pp. 97-109, 1983.

[9]   X. Bi and Q. Zhu, "Fluid-structure Investigation of a squid-Inspired swimmer," *Phys. Fluids,* vol. 31, p. 101901, 2019.

[10] E. Anderson and E. DeMont, "The mechanics of locomotion in the squid Liligo Pealei: locomotion function and unsteady hydrodynamics of the jet and intrementle pressure," *J. Exp. Biol.,* vol. 203, pp. 2851-2863, 2000.

[11] E. Anderson and M. Grosenbaugh, "Jet flow in steadily swimming adult squid," *J. Exp. Biol.,* vol. 208, pp. 1125-1146, 2005.

[12] X. Bi and Q. Zhu, "Dynamics of a squid-inspired swimmer in free swimming," *Bioinsp. Biomim.,* vol. 15, p. 016005, 2019.

[13] H. Neumeister, B. Ripley and W. Gilly, "Effects of temperature on escape jetting in the squid Loligo Opalescens," *J. Exp. Biol.,* vol. 203, pp. 547-557, 2000.

[14] K. Muramatsu, J. Yamamoto, T. Abe, K. Sekiguchi, N. Hoshi and Y. Sakurai, "Oceanic squid do fly," *Mar. Biol.,* vol. 160, pp. 1171-1175, 2013.

[15] R. O'Dor, J. Stewart, W. Gilly, J. Payne, T. Borges and T. Thys, "Squid rocket science: How squid launch into air," *Deep-Sea Research II,* vol. 95, pp. 113-118, 2013.

[16] R. O'Dor, "How squid swim and fly," *Can. J. Zool.,* vol. 91, pp. 413-419, 2013.

[17] R. Alexander, "Swimming," in *Mechanics and energetics of animal locomotion*, R. Alexander and G. Goldspink, Eds., London, Chapman and Hall, 1977, pp. 222-248.

[18] R. O'Dor and D. Webber, "The constraints on cephalopods: why squid aren't fish," *Can. J. Zool.,* vol. 64, pp. 1591-1605, 1986.

[19] J. Vidler, Fish swimming, London: Chapman and Hall, 1993.

[20] D. Webber and R. O'Dor, "Respiratory metabolism and swimming performance of the squid, lllex illecebrosus," *Northwest Atl. Fish Organ. Sci. Counc. Stud.,* vol. 9, pp. 133-138, 1985.

[21] R. O'Dor and D. Webber, "Invertegrate athletes: Trade-offs between transprt efficiency and power density in cephalopod evolution," *J. Exp.Biol.,* vol. 160, pp. 93-112, 1991.

[22] P. Linden and J. Turner, "`Optimal' vortex rings and aquatic propulsion mechanisms," *Proc. R. Soc. Lond. B,* vol. 271, pp. 647-653, 2004.

[23] W. Johnson, P. Soden and E. Trueman, "A study in jet propulsion: an analysis of the motion of the squid, Loligo vulgaris," *J. Exp. Biol.,* vol. 56, pp. 155-165, 1972.

[24] I. Bartol, P. Krueger, W. Stewart and J. Thompson, "Hydrodynamics of oulsed jetting in juvenile and adult brief squid Lolliguncula brevis: evidence of multi jet `modes' and their implications for propulsive efficiency," *J. Exp. Biol.,* vol. 212, pp. 1889-1903, 2009.

[25] D. Staaf, W. Gilly and M. Denny, "Aperture effects in squid jet propulsion," *J. Exp. Biol.,* vol. 217, pp. 1588-1600, 2014.

[26] H. Jiang, "Numerical simulation of self-propelled steady jet propulsion at intermediate Reynolds numbers: effects of orifice size on animal jet propulsion," *Fluids,* vol. 6, p. 230, 2021.

[27] H. Jiang, J. Costello and S. Colin, "Fluid dynamics and efficiency of colonial swimming via multijet propulsion at intermediate Reynolds numbers," *Phys. Rev. Fluids,* vol. 6, p. 031103, 2021.

[28] X. Bi and Q. Zhu, "Efficiency of pulsed-jet propulsion via thrust-drag decomposition," *Phys. Fluids,* vol. 33, p. 071902, 2021.

[29] X. Bi and Q. Zhu, "Free swimming of a squid-inspired axisymmetric system through jet propulsion," *Bioinsp. Biomim.,* vol. 16, p. 066023, 2021.

[30] M. Gharib, E. Rambod and K. Shariff, "A universal time scale for vortex ring formation," *J. Fluid Mech.,* vol. 360, pp. 121-140, 1998.

[31] M. Rosenfeld, E. Rambod and M. Gharib, "Circulation and formation number of lamina vortex rings," *J. Fluid Mech.,* vol. 376, pp. 297-318, 1998.

[32] L. Gao, X. Wang, S. Yu and M. Chyu, "Development of the impulse and thrust for laminar starting jets with finite discharged volume," *J. Fluid Mech.,* vol. 902, p. A27, 2020.

[33] P. Krueger and M. Gharib, "Thrust augmentation and vortex ring evolution in a fully pulsed jet," *AIAA J.,* vol. 43, no. 4, pp. 792-801, 2005.

[34] P. Linden and J. Turner, "The formation of `optimal' vortex rings, and the efficiency of propulsion devices," *J. Fluid Mech.,* vol. 427, pp. 61-72, 2001.

22

[35] P. Linden and J. Turner, "`Optimal' vortex rings amd aquatic propulsion mechanisms," *Proc. R. Soc. Lond. B,* vol. 271, pp. 647-653, 2004.

[36] C. York, I. Bartol, P. Krueger and J. Thompson, "Squids use multiple escape jet patterns throughout ontogeny," *Biology Open,* vol. 9, p. bio054585, 2020.

[37] W. Stewart, I. Bartol and P. Krueger, "Hydrodynamic fin function of brief squid, Lolliguncula Brevis," *J. Exp. Biol.,* vol. 213, pp. 2009-2004, 2010.

[38] P. Krueger and M. Gharib, "The significance of vortex ring formation to the impulse and thrust of a starting jet," *Phys. Fluids.,* vol. 15, no. 5, pp. 1271-1281, 2003.

[39] P. Krueger, "The significance of vortex ring formation and nozzle exit over-pressure to pulsatile jet propulsion," California Institute of Technology, Pasadena, California, 2001.

[40] A. Moslemi and P. Krueger, "The effect of Reynolds number on the propulsive efficiency of a biomorphic pulsed-jet underwater vehicle," *Bioinsp. Biomim.,* vol. 6, p. 026001, 2011.

[41] C. Palacios-Morales and R. Zenit, "Vortex ring formation for low Re numbers," *Acta Mech.,* vol. 224, pp. 383-397, 2012.

[42] X. Bi and Q. Zhu, "Pulset-jet propulsion via shape deformation of an axisymmetric swimmer," *Phys. Fluids,* vol. 32, p. 081902, 2020.

[43] P. Krueger, J. Dabiri and M. Gharib, "Vortex ring pinchoff in the prescence of simultaneously initiated uniform background co-flow," *Phys. Fluids,* vol. 15, no. 7, pp. L49-L52, 2003.

[44] J. Dabiri and M. Gharib, "Delay of vortex ring pincho by an imposed bulk counterflow," *Phys. Fluids,* vol. 16, no. 4, p. L28, 2004.

[45] H. Jiang and M. Grosenbaugh, "Numerical simulation of vortex ring formation in the presence of background flow with implications for squid propulsion," *Theor. Comput. Fluid Dyn.,* vol. 20, no. 2, pp. 103-123, 2006.

[46] M. Krieg and K. Mohseni, "Modeling circulation, impulse and kinetic energy of starting jets with non-zero radial velocity," *J. Fluid Mech.,* vol. 719, pp. 488-526, 2013.

[47] X. Bi and Q. Zhu, "Effect of nozzle geometry on the performance of pulsed-jet propulsion at low Reynolds number," *J. Fluids Struc.,* vol. 107, p. 103402, 2021.

[48] A. Athanassiadis and D. Hart, "Effects of multijet coupling on propulsive performance in underwater pulsed jets," *Phys. Rev. Fluids,* vol. 1, p. 034501, 2016.

[49] A. Athanassiadis, "Parallel pulsed jets for precise underwater propulsion," Massachusstes Institute of Technology, Cambridge, MA, 2016.

[50] K. Sutherland and D. Weihs, "Hydrodynamic advantages of swimming by salp chains," *J. R. Soc. Interface,* vol. 14, p. 20170289, 2017.

[51] P. Saffman, "The self-propulsion of a deformable body in a perfect fluid," *J. Fluid Mech.,* vol. 28, pp. 385-389, 1967.

[52] S. Chidress, N. Vandengerge and J. Zhang, "Hovering of a passive body in an oscillating airflow," *Phys. Fluids,* vol. 18, p. 117103, 2006.

[53] S. Spagnolie and M. Shelley, "Shape-changing bodies in fluid: hovering, ratcheting, and bursting," *Phys. Fluids,* vol. 21, p. 013103, 2009.

[54] S. Childress, S. Spagnolie and T. Tokieda, "A bug on a raft: recoil locomotion in a viscous fluid," *J. Fluid Mech.,* vol. 669, pp. 527-556, 2011.

[55] G. Weymouth and M. Triantafyllou, "Ultra-fast escepe of a deformable jet-propelled body," *J. Fluid Mech.,* vol. 721, pp. 367-385, 2013.

[56] S. Steele, G. Weymouth and M. Triantafyllou, "Added mass energy recovery of octopus-inspired shape change," *J. Fluid Mech.,* vol. 810, pp. 155-174, 2017.

[57] F. Giorgio-Serchi and G. Weymouth, "Drag cancellation by added-mass pumping," *J. Fluid Mech.,* vol. 798, p. R3, 2016.

[58] G. Weymouth and F. Giorgio-Serchi, "Analytic modeling of a size-changing swimmer," in *IUTAM Symposium on Critical flow dynamics involving moving/deformable structures with design applications*, Santorini, Greece, 2018.

[59] X. Bi and Q. Zhu, "Numerical investigation of cephalopod-inspired locomotion with intermittent bursts," *Bioinsp. Biomim.,* vol. 13, p. 056005, 2018.

[60] C. Christianson, Y. Cui, M. Ishida, X. Bi, Q. Zhu, G. Pawlak and M. Tolley, "Cephalopod-inspired robot capable of cyclic jet propulsion through shape change," *Bioinsp. Biomim.,* vol. 16, p. 016014, 2020.

[61] F. Renda, F. Giorgio-Serchi, F. Boyer and C. Laschi, "Modelling cephalopod-inspired pulsed-jet locomotion for underwater soft robots," *Bioinsp. Biomim.,* vol. 10, p. 055005, 2015.

[62] F. Giorgio-Serchi, A. Arienti and C. Laschi, "Underwater soft-bodied pulsed-jet thrusters: actuaor odeling and performance profiling," *The International Journal of Robotics Research,* vol. 35, no. 11, pp. 1308-1329, 2016.

[63] Q. Zhu, M. Wolfgang, D. Yue and M. Triantafyllou, "Three-dimensional flow structures and vorticity control in fish-like swimming," *J. Fluid Mech.,* vol. 468, pp. 1-28, 2002.

24

[64] Y. Luo, Q. Xiao, Q. Zhu and G. Pan, "Jet propulsion of a squid-inspired swimmer in the presence of background flow," *Phys. Fluids,* vol. 33, p. 031909, 2021.

[65] J. Carter, J. Soria and T. Lim, "The interaction of the piston vortex with a piston-generated vortex ring," *J. Fluid Mech.,* vol. 499, pp. 327-343, 2004.

[66] Y. Luo, Q. Xiao, Q. Zhu and G. Pan, "Pulsed-jet propulsion of a squid-inspired swimmer at high Reynolds number," *Phys. Fluids,* vol. 32, p. 111901, 2020.

[67] T. Hou, X. Yang, T. Wang, J. Liang, S. Li and Y. Fan, "Locomotor transition: how squid jet from water to air," *Bioinspir. Biomim.,* vol. 15, p. 036014, 2020.

[68] M. Krieg and K. Mohseni, "Thrust characterization of a bioinspired vortex ring thruster for locomotion of underwater robots," *IEEE J. Ocean Engr.,* vol. 33, no. 2, pp. 123-132, 2008.

[69] A. Moslemi and P. Krueger, "Propulsive efficiency of a niomorphic pulsef-jet underwater vehicle," *Bioinsp. Biomim.,* vol. 5, p. 036003, 2010.

[70] L. Ruiz, R. Whittlesey and J. Dabiri, "Cortex-enhanced propulsion," *J. Fluid Mech.,* vol. 668, pp. 5-32, 2011.

[71] P. Linden, "The efficiency of pulsed-jet propulsion," *J. Fluid Mech.,* vol. 668, pp. 1-4, 2011.

[72] R. Zufferey, A. Ancel, A. Farinha, R. Siddall, S. Armanini, M. Nasr, R. Brahmal, G. Kennedy and M. Kovac, "Consecutive aquatic jump=gliding with water-reactive fuel," *Science Robotics,* vol. 4, p. eaax7330, 2019.

[73] T. Hou, X. Yang, H. Su, B. Jiang, L. Chen, T. Wang and J. Liang, "Design and experiments of a squid-like aquatic-aerial vehicle with soft morphing fins and arms," in *International Conference on Robotics and Automation*, 2019.

[74] C. Tang, W. Ma, B. Li, M. Jin and H. Chen, "Cephalopod-inspired swimming robot using dielectric elastomer synthetic jet actuator," *Adv. Eng. Mater.,* vol. 22, p. 1901130, 2020.

[75] F. Giorgio-Serchi, A. Arienti, I. Baldili and C. Laschi, "An elastic pulsed-jet thruster for soft unmanned underwater vehicles," in *IEEE Int. Conf. Robot. Autom*, 2013.

[76] F. Giorgio-Serchi, A. Arienti and C. Laschi, "Biomimetic vortex propulsion: toward the new paradigm of soft unmanned underwater vehicles," *IEEE/ASME Trans. Mechatron.,* vol. 18, pp. 484-493, 2013.

[77] G. Weymouth, V. Subramaniam and M. Triantafyllou, "Ultra-fast escape maneuver of an octopus-inspired robot," *Bioinsp. Biomim.,* vol. 10, p. 016016, 2015.

[78] F. Giorgio-Serchi, A. Lidtke and G. Weymouth, "A soft aquatic actuator for unsteady peak power amplification," *IEEE/ASME Trans. Mechatron.,* vol. 23, no. 6, pp. 2968-2973, 2018.

[79] N. Xu, "Squid-inspired robots perform swimmingly," *Sci. Robot.,* vol. 6, p. eabf4301, 2021.

[80] Z. Yang, D. Chen, D. Levine and C. Sung, "Origami-Inspired robot that swims via jet propulsion," *IEEE Robotics and Automation Letters,* vol. 6, no. 4, pp. 7145-7152, 2021.

[81] T. Bujard, F. Giorgio-Serchi and G. Weymouth, "A resonant squid-inspired robot unlocks biological propulsive efficiency," *Sci. Robot.,* vol. 6, p. eabd2971, 2021.

[82] X. Bi and Q. Zhu, "Role of internal flow in squid-inspired jet propulsion," *Phys. Fluids,* vol. 34, no. 3, p. 031906, 2022.

[83] Q. Bone and E. Trueman, "Jet propulsion in salps (tunicata: Thaliacea)," *J. Zool. Lond.,* vol. 201, no. 4, pp. 481-506, 1983.

[84] L. Madin, "Aspects of jet propulsion in salps," *Can. J. Zool.,* vol. 68, no. 4, pp. 765-777, 1990.

[85] T. Wang, A. Lidtke, F. Giorgio-Serchi and G. Weymouth, "Manoeuvring of an aquatic soft robot using thrust-vectoring," in *2nd IEEE International Conference on Soft Robotics (RoboSoft)*, Seoul, Korea, 2019.

[86] M. Philen, "SMA active fiber pumps inspired by the squid mantle," *Bioinsp. Biomim.,* vol. 16, p. 026017, 2021.

[87] R. Kelso, T. Lim and A. Perry, "An experimental study of round jets in cross-flow," *J. Fluid Mech.,* vol. 306, pp. 111-144, 1996.

[88] T. Lim, T. New and S. Luo, "On the development of large-scale structures of a jet normal to a cross flow," *Phys. Fluids,* vol. 13, p. 770, 2001.

[89] T. New, T. Lim and S. Luo, "Elliptic jets in cross-flow," *J. Fluid Mech.,* vol. 494, pp. 119-140, 2003.

[90] T. New, T. Lim and S. Luo, "Effects of jet velocity profiles on a round jet in cross-flow," *Exp. Fluids,* vol. 40, pp. 859-875, 2006.